

1 *Submitted to American Mineralogist - Special Collection "Geochemical Transport Processes"*
2 *Revision II – submitted August 2014*

3
4 **Timescales of exhumation and cooling inferred by kinetic modelling: An**
5 **example using a lamellar garnet pyroxenite from the Variscan**
6 **Granulitgebirge, E Germany**

7
8 Thomas Müller¹, Hans-Joachim Massonne², and Arne P. Willner^{1,2}

9
10 ¹Institut für Geologie, Mineralogie & Geophysik, Ruhr-Universität Bochum, D-44801
11 Bochum

12 ²Institut für Mineralogie und Kristallchemie; Universität Stuttgart; D-70174 Stuttgart,
13 Germany

14
15 *Keywords:*

16 diffusion, mineral growth, garnet, clinopyroxene, contact metamorphism, kinetics, timescales,
17 reaction mechanism, reaction rate

18
19 *Corresponding authors present address:*

20 Thomas Müller; Ruhr-Universität Bochum, Universitätsstraße 150, Gebäude NA03/586; D-
21 44801 Bochum, Germany; Email: thomas.mueller-1@rub.de

22
23 **Abstract**

24 We present a numerical modeling approach to infer timescales of the exhumation and cooling
25 history recorded in the chemical composition of minerals in a garnet pyroxenite from the
26 Granulitgebirge, Saxony/Germany. The studied sample contains remarkable exsolution
27 textures from former megacrysts that produced up to mm-wide, alternating lamellae of garnet
28 (grt) and clinopyroxene (cpx). Compositional profiles of major and minor elements measured
29 with the electron microprobe perpendicular to the grt-cpx interfaces reveal systematic zoning
30 patterns for Fe, Mg, Al, Si, Cr, Ti in clinopyroxene and Ca, Fe, Mg, Mn in garnet,
31 respectively. In addition to simple thermal modelling that is used to constrain the conditions
32 of emplacement of the Granulitgebirge Massif at shallow crustal levels, we combine
33 thermodynamic data with a numerical finite difference scheme that simulates growth and
34 simultaneous diffusive exchange between garnet and clinopyroxene along a virtual cooling
35 path. The latter model assumes local equilibrium at the interface. Diffusive fluxes are
36 constrained by mass balance. It is shown that zoning patterns such as Fe-Mg exchange
37 between garnet and clinopyroxene can be used to extract cooling rates and thus timescales of
38 exhumation, while the profiles for the minor elements are provisionally related to the growth
39 history of the lamellae. Furthermore, zoning profiles in the lamellae can only be reproduced
40 with ultrahigh cooling rates similar to contact metamorphic conditions. This in turn, suggests
41 that the massif was emplaced at temperatures above 900°C in agreement with the observed
42 spatial extent of a contact aureole within low-grade metasedimentary rocks surrounding the
43 granulite massif as predicted by thermal modeling. Exhumation of the massif without cooling
44 below 900°C requires an exhumation rate of several cm/yr. Thus, we propose an almost

45 isothermal exhumation period of ~1Ma followed by isobaric cooling from 900 to 600°C
46 within less than 10 ka.
47

48 **Introduction**

49 Metamorphic textures and mineral compositions are records of complex geodynamic
50 processes such as subduction, orogenesis or exhumation. Determination of pressure and
51 temperature conditions at various stages is one of the key tools to constrain the evolution of
52 rock units on a larger scale. Commonly, thermodynamic calculations are used to infer P-T
53 conditions based on observed phase assemblages and mineral compositions. The use of
54 thermodynamic data is founded on the assumption that phases in a given sample are
55 effectively able to adjust their composition up to a certain point in time and remain perfectly
56 closed afterwards, i.e. without any further exchange reaction on the retrograde path.
57 Especially in medium to high grade metamorphic rocks this assumption is questionable as
58 virtually every system, evolving along a T-t path, is subject to diffusive re-equilibration to
59 different extents. In the last decade, an increasing number of studies investigated non-
60 equilibrium aspects with regard to textural and compositional records in rocks on various
61 scales (e.g., Roselle et al., 1997; Mueller et al., 2004; Gaidies et al., 2008a; Gaidies et al.,
62 2008b; Mueller et al., 2008; Caddick et al., 2010; Mueller et al., 2010; Gaidies et al., 2011).
63 Rather than a limitation, the incomplete readjustment of mineral compositions during
64 metamorphism should be regarded as an additional source of information on the mechanism
65 and rates of processes, such as element / isotope exchange during large scale geodynamic
66 processes with significantly changing P-T conditions (see also review by Mueller et al., 2010).
67 Lasaga (1983) published a landmark paper in which he used the temperature dependent ability
68 of diffusive compositional adjustment to infer exhumation rates based on the cooling history
69 recorded in diffusion profiles of elements in minerals which led to the concept of
70 “geospeedometry”. While the original focus of this approach was on exhumation rates, i.e. the

71 determination of speed in mm/year, it has also often been misleadingly used to estimate
72 timescales of igneous and metamorphic processes (for a detailed description see review by
73 Costa et al., 2008). However, the concept of the determination of rates and durations of
74 processes for isothermal and non-isothermal histories can successfully be applied if the
75 relevant transport parameters, e.g. diffusion coefficients and information on other factors
76 controlling the diffusive flux (e.g. grain size, modal abundance) are available. As a
77 consequence, cooling histories of metamorphic terrains have been determined using this
78 kinetic modeling approach (Lasaga et al., 1977; Spear and Florence, 1992; Ducea et al., 2003;
79 Trepmann et al., 2004; Hauenberger et al., 2005). Element exchange driven by diffusion is
80 largely dependent on temperature, which directly relates the applicability of geospeedometry
81 and geothermobarometry to the concept of diffusive closure of a mineral (Dodson, 1973;
82 Dodson, 1986; Ganguly and Tirone, 1999). However, a complete description of the dynamic
83 system governing the geochemical fluxes, in turn, allows evaluating whether mineral
84 compositions are reset during heating, cooling and/or decompression and if so, to which
85 extent. For example, the effect of mixed-volatile reaction, volume diffusion, and exsolution
86 has been studied to successfully reproduce variations in measured calcite-dolomite
87 thermometric data in contact metamorphic settings (Mueller et al., 2008). Recently, the Fe-Mg
88 interdiffusion data for various ferromagnesian minerals such as garnet (Borinski et al., 2012),
89 spinel (Liermann and Ganguly, 2002), clinopyroxene (Mueller et al., 2013), and
90 orthopyroxene (Ganguly and Tazzoli, 1994) have been determined. Knowledge of these
91 kinetic parameters in turn was used to evaluate the effect on the element distribution and thus
92 on apparent thermometric data for typical cosmochemical and geological settings (Ganguly et
93 al., 2013; Mueller et al., 2013).

94 In this paper, we use numerical models of kinetically controlled element exchange
95 between co-existing garnet (grt) and clinopyroxene (cpx) exsolution lamellae to study the
96 effect and timescales of diffusive compositional adjustment during a cooling and exhumation

97 event. Such lamellae occur in an ultrabasic rock intercalated within a complex of high
98 pressure granulite in the Variscan Granulitgebirge (Saxony/Germany). This metamorphic
99 complex is a suitable example for two reasons: (1) the geological setting is simple enough to
100 place solid constraints on the geometry, different lithologies, and tectonic setting (Fig. 1 and
101 Reinhardt and Kleemann, 1994) and (2) there are a large number of studies which focused on
102 the P-T evolution using exchange reactions and thermodynamic calculations (Roetzler and
103 Romer, 2001; Massonne and Bartsch, 2002; Roetzler et al., 2004; Hagen et al., 2008; Roetzler
104 et al., 2008; Schmaedicke et al., 2010) in addition to geochronological data that provide
105 independent estimates for the timescale of the exhumation process (von Quadt, 1993; Kroener
106 et al., 1998; Romer and Roetzler, 2001; Roetzler and Romer, 2010). It is shown here that a
107 combination of equilibrium phase petrology and modeling of mass and heat transport can
108 improve the reconstructed P-T-t exhumation path. Finally, the new results are discussed in the
109 context of a large scale geodynamic exhumation model comparing previous petrological
110 findings.

111

112 **Geological settings and previously derived P-T-t evolution of the Granulitgebirge**

113 The Variscan orogen of Europe formed by collision of the palaeocontinents Laurussia
114 and Gondwana in the Late Palaeozoic. Many researchers assume that Gondwana-derived
115 terrains collided with Laurussia first before Gondwana came in contact with Laurussia (e.g.,
116 Kroner and Romer, 2013). The eastern part of this orogen is represented by the Bohemian
117 Massif, a collage of diverse basement blocks, which include units of high temperature, high to
118 ultrahigh pressure metamorphic rocks from the root of the collisional orogen. These rock
119 assemblages include garnet peridotite, eclogite, high pressure mafic and felsic granulite as
120 well as related quartzofeldspathic rocks with a wide range of maximum P-T estimates [700° to
121 1100°C, 0.4 to 4.5 GPa (for summary see Massonne, 2011)]. The ages of high-pressure
122 metamorphism in the Bohemian Massif are bimodal (Kroener and Willner, 1998): 400-380

4

123 Ma in the Gory Sowie, Tepla Barrandian Unit, and Münchberg Complex and 350-335 Ma in
124 the Erzgebirge, Granulitgebirge, Snieznik, and Gföhl Unit (Fig. 1a). Evolution and
125 mechanism of exhumation of these high pressure rocks are still a matter of debate (e.g.,
126 Willner et al., 2002; Kroner and Goerz, 2010).

127 The Granulitgebirge in Saxony (Germany) in the northern part of the Bohemian Massif
128 represents a key unit for the younger high-pressure event, where geodynamic processes were
129 studied in detail within a rather small area. The Granulitgebirge forms an oval-shaped dome
130 structure composed of high-pressure felsic granulite including lenses of mafic granulite and
131 garnet peridotite (Werner, 1987; Roetzler et al., 1992; Reinhardt and Kleemann, 1994;
132 Roetzler and Romer, 2010). Protoliths of the granulites are Cambro-Ordovician igneous rocks
133 with calcalkaline and tholeiitic affinities (Werner, 1987; Kroener et al., 1998). The contact of
134 the Granulitgebirge to the surrounding rocks, which are low-pressure siliciclastic
135 metasediments of early Palaeozoic to late Devonian age, is represented by a major extensional
136 detachment zone. This shear zone comprises (1) the rim of the granulite complex, (2)
137 dismembered slivers of medium-pressure garnet-cordierite gneiss and ophiolitic rocks, and (3)
138 the lower part of the metasedimentary cover, and it shows a top-to-SE tectonic transport
139 (Roetzler et al., 1992; Reinhardt and Kleemann, 1994). Various peak P-T conditions were
140 estimated for the felsic and mafic granulites: >1 GPa, >800 °C (Grew, 1986; Roetzler et al.,
141 1992), 2.2-2.3 GPa, >1000 °C (Roetzler and Romer, 2001; Roetzler et al., 2004; Hagen et al.,
142 2008; Roetzler et al., 2008; Roetzler and Romer, 2010) and 1.4 GPa, > 800 °C (Massonne,
143 2006). The P-T estimates for the garnet peridotite and associated garnet pyroxenite and
144 eclogite are in the range 1.9-3.3 GPa, 1000-1070 °C (Roetzler and Romer, 2001; Massonne
145 and Bartsch, 2002; Schmaedicke et al., 2010). Later equilibration stages in the granulite
146 during the exhumation were estimated to 0.9-0.95 GPa, 890-940 °C (Roetzler and Romer,
147 2001), 1.0-1.05 GPa, 940-980 °C [symplectite stage (Roetzler et al., 2008)] and 0.25 GPa, 740
148 °C [final emplacement stage (Roetzler et al., 2004)]. The age of the peak pressure conditions

149 was constrained by dating of zircon (341.5 ± 0.8 Ma) and titanite (342 ± 0.8 Ma) with the U/Pb
150 system (Romer and Roetzler, 2001). The obtained data agree with earlier zircon ages derived
151 by von Quadt (1993) and Kroener et al. (1998). From the study of the garnet-cordierite gneiss,
152 a decompression-heating path of 0.65 GPa, 730 °C to 0.5 GPa, 790°C was invoked by
153 Roetzler & Romer (2010). These authors interpreted this partial P-T path as being due to heat
154 transfer from the rising granulite.

155 The low-pressure metasediments (phyllite) surrounding the granulites show a
156 progressive metamorphic zonation from very low grade metamorphic conditions towards
157 incipient migmatization near the contact to the granulites at a depth corresponding to 0.2-0.3
158 GPa (Roetzler et al., 1992; Reinhardt and Kleemann, 1994). Subsequent growth of chlorite,
159 andalusite, staurolite, cordierite, garnet, and sillimanite is observed in these metasediments
160 (schist mantle). This ~1-3 km wide halo around the granulite complex is interpreted as the
161 result of heating after emplacement of this complex during exhumation (Roetzler et al., 1992;
162 Reinhardt and Kleemann, 1994; Roetzler and Romer, 2010). Rb/Sr ages of white mica in the
163 low-pressure metasediments can be grouped into three categories according to Roetzler &
164 Romer (2010): (1) ages of 348.6 ± 3.5 Ma and 349.4 ± 3.5 Ma at more than 600 m from the
165 contact reflect the age of regional metamorphism of the sediments prior to emplacement of the
166 granulites; (2) an age of 337.6 ± 3.6 in the garnet-cordierite gneiss at the contact overlaps with
167 the age of the peak of metamorphism in the granulite complex and is interpreted as the age of
168 its juxtaposition with the granulite complex; (3) an age of 333.6 ± 4.2 Ma in the schists at the
169 contact is consistent with Ar-Ar ages of white mica of 334.2 ± 1.9 Ma and 332.6 ± 4 Ma
170 (Werner and Reich, 1997) in these schists and a Pb-Pb single-zircon evaporation age of
171 333.1 ± 1.0 Ma for a concordant granite intrusion into the schists (Kroener et al., 1998). The
172 latter ages are interpreted as the time of the arrival of the granulite complex at shallow crustal
173 depth and the formation of the contact metamorphic halo (Roetzler and Romer, 2010). The
174 determined time interval for the exhumation of ~7 Myrs results in an exhumation rate of 7-13

175 mm/yr and a cooling rate of 40-70 °C/Myr (Roetzler and Romer, 2010). This very rapid
176 extensional unroofing of the granulite complex from the root of a thickened crust (Reinhardt
177 and Kleemann, 1994) is matched by comparable exhumation rates and mechanisms of high-
178 pressure rocks in the Erzgebirge in the south (Willner et al., 2000; Willner et al., 2002;
179 Massonne et al., 2007). Extensional unroofing in an “exhumation channel” is thought to be
180 balanced by concomitant stacking at depth during ongoing convergence. Delamination of the
181 lithospheric mantle was envisaged as primary cause for the rapid exhumation of the 350-335
182 Ma high-pressure rocks from the crustal root throughout the Bohemian Massif, where a
183 thickened crust was likely maintained since the time of collision at 400-380 Ma (Massonne
184 and O'Brien, 2003; Massonne, 2006), when the older high-pressure units of the Bohemian
185 Massif originated. Other geodynamic models invoke intracontinental subduction (Kroner and
186 Goerz, 2010; Kroner and Romer, 2013) or considerable crustal stacking after deep crustal
187 subduction (O'Brien, 2008).

188

189 **Sample description, mineral composition and origin of lamellar megacrysts**

190 We studied a garnet pyroxenite from the abandoned serpentinite quarry at the village
191 of Reinsdorf, Saxony (Germany). The garnet pyroxenite, which was first described by
192 Hentschel (1937) and originally named as “Eklogit von Gilsberg“, forms several centimeter to
193 decimeter thick, boudinaged layers in the serpentinite body. These layers are parallel to each
194 other. In some instances, alternating lamellae of garnet and clinopyroxene are discernable in
195 the garnet pyroxenite (Fig. 2). Such domains of lamellar fabric are surrounded by more or less
196 equigranular domains, which consist of mm-sized grains of garnet and clinopyroxene
197 representing an equilibrium texture (Fig. 2). Both types of fabric can occur in homogeneous
198 domains of several cm³ in our sample. The equilibrium texture was the result of
199 recrystallization of the lamellae proven by intermediate stages (e.g. curved and partially
200 recrystallized lamellae as the result of deformation) between both types of fabric (Massonne

7

201 and Bautsch, 2002). The garnet lamellae are topotaxially intergrown with clinopyroxene [cpx:
202 (100)cpx//(110)grt and [001]cpx//[100]grt as well as (100)cpx//(100)grt and
203 [001]cpx//[110]grt (Reiche and Bautsch, 1984; Jekosch and Bautsch, 1991)]. Therefore, the
204 lamellar texture was interpreted to be the result of exsolution of garnet from clinopyroxene
205 (Reiche and Bautsch, 1985) because of the dominance of clinopyroxene lamellae [vol.%
206 cpx/grt = 7:3, (Massonne and Bautsch, 2002)]. As the lamellae can extend parallel over
207 several cm, the invoked clinopyroxene originally occurred as megacrysts up to 10 cm in size
208 forming once monomineralic layers in the exposed, now serpentinized mantle fragment.

209 Especially thick garnet lamellae without visible symplectites [composed of
210 orthopyroxene, spinel, clinopyroxene and anorthite-rich plagioclase (Massonne and Bautsch,
211 2002)] were selected for detailed compositional profiles perpendicular to the interface
212 between lamellae. Electron microprobe measurements have been performed using a Cameca
213 SX 100 at Universität Stuttgart. Garnet and clinopyroxene composition have been analyzed at
214 15 kV and a beam current of 30 or 40 nA. A total of ten profiles for adjacent grt-cpx lamellae
215 have been measured at different positions within the limits of a former megacryst. No
216 significant difference can be observed and representative compositional profiles are shown in
217 figure 3. Measured profiles reveal almost flat, but often slightly zoned patterns with
218 increasing pyrope and almandine and decreasing grossular component from the garnet center
219 towards the interface (Fig. 3), and almost no zoning of any major element from core to rim
220 can be observed in the adjacent clinopyroxene (Fig. 3; see also Massonne and Bautsch, 2002).
221 Spatially resolved minor element compositions show an increase in concentration of Cr, V
222 and Ti towards the clinopyroxene rim. In contrast, no zoning for Cr and V can be observed in
223 the garnet, which is also nearly free of titanium (Fig. 3).

224 In a previous study, Massonne and Bautsch (2002) determined the original megacryst
225 composition on the basis of the compositions of the slightly chemically zoned clinopyroxene
226 and garnet and their abundance. They concluded that the megacrysts were either Al-rich

227 clinopyroxenes formed at about 1.7 GPa and 1400°C or Ca-majoritic garnets from an upper
228 portion of the mantle transition zone. The question of the original host phase, i.e. whether
229 garnet exsolved from clinopyroxene or vice versa, has important consequences for the
230 reconstruction of the P-T evolution as argued by Massonne and Bartsch (2002). These authors
231 used bulk rock trace element compositions to argue for a majoritic garnet to be the former
232 host phase. In contrast, Reiche and Bartsch (1985) proposed cpx as the original phase based
233 on the higher abundance of cpx compared to garnet. Roetzler and Romer (2010) argued that
234 Al-rich spinel inclusions measured in garnet crystals of the matrix support the case of a cpx
235 host. In fact, it is not essential to the purposes of this paper to determine the original host
236 phase, but the spatially resolved compositional trace element profiles potentially contain the
237 information needed to answer this question. For example, the virtually Ti-free garnet and the
238 visible Ti-zoning in clinopyroxene (Fig. 3) could be interpreted as the consequence of
239 titanium accumulation in clinopyroxene during the growth of the garnet lamella in which Ti is
240 rather incompatible. Consequently, back diffusion of Ti into the residual clinopyroxene
241 lamellae would then lead to the observed compositional profile as observed in other studies
242 for Nb in rutile after reaction to titanite (Lucassen et al., 2011; Cruz-Urbe et al., 2014).

243

244 **Numerical modeling**

245 Peak metamorphic conditions are typically determined with geothermobarometers, for
246 example the temperature dependent exchange of elements between two minerals (e.g. Fe-Mg
247 between garnet and biotite). Based on thermodynamics, corresponding calculations constrain
248 equilibrium between minerals that is the direct record of intrinsic, external variables such as
249 temperature, pressure or a partition coefficient. A very important assumption for the
250 interpretation of this concept to metamorphic rocks is that minerals are thought to adjust their
251 composition infinitely fast according to the external conditions at least during prograde
252 metamorphism, which includes formation of new minerals by net transfer reaction,

9

253 recrystallization and/or fast diffusive homogenization at elevated temperatures. In contrast,
254 retrograde adjustment of mineral compositions during cooling is often interpreted to be
255 sluggish which has led many researchers to the erroneous interpretation that only mineral rim
256 compositions are affected by retrograde element exchange whereas core compositions are
257 likely to reflect peak metamorphic conditions. The later assumption has been shown to depend
258 on a number of parameters such as cooling rate, grain size, modal abundances, which all
259 determine the transport properties of elements along grain boundaries and within crystals and
260 thus the effective flux of elements (Fisher, 1978; Ganguly and Tirone, 1999; Dohmen and
261 Chakraborty, 2003; Mueller et al., 2010). Thus, it is necessary to evaluate which part of the
262 thermal history is recorded in the chemical zoning pattern for a given mineral pair and set of
263 parameters given above. Dodson (1973) developed a formulation to compute the so-called
264 “closure temperature” being the mean temperature at which declining diffusion rates preclude
265 significant exchange of elements by diffusion at a given cooling rate and grain size under the
266 assumption of a simple mineral geometry and effectively infinite reservoir to exchange with.
267 Later, some modifications allowed the spatial resolution of the closure temperature for
268 different parts of a crystal (e.g., Dodson, 1986; Ganguly and Tirone, 1999). However, in the
269 present case, interdiffusion rates of Fe-Mg in clinopyroxene (Mueller et al., 2013) and garnet
270 (Borinski et al., 2012) are very similar, i.e. the assumption of an effectively infinite reservoir
271 and thus the above formulation cannot be used to evaluate the compositional resetting of a
272 cpx-grt pair during cooling. In recent studies, Ganguly et al. (2013) and Mueller et al. (2013)
273 stated that there is no analytical solution for this problem and they developed a 1-D numerical
274 model for a polythermal diffusive element exchange between two phases without net mass
275 transfer under isobaric conditions using a temperature dependent partition coefficient. The
276 model of Mueller et al. (2013), specifically focused on the Fe-Mg exchange between
277 ferromagnesian mineral pairs (spinel, garnet, olivine, ortho- and clinopyroxene). Modeling

278 results revealed that for most geologically relevant conditions the mineral pairs efficiently
279 adjust their chemical composition above 1000-1100 °C independent of the cooling rate.

280 In this study, we extended the simple polythermal diffusive element exchange model
281 to incorporate the effect of exhumation (i.e., decompression) and mineral growth (i.e., net
282 mass transfer) and applied this to the grt-cpx lamellae in our sample. The length of the
283 modeled compositional profiles perpendicular to the interface between the lamellae are
284 negligible compared to the extent of the lamellae parallel to the interface which justifies the
285 application of the 1-D model geometry excluding additional element fluxes in a second or
286 even third dimension. For both adjacent lamellae we solved the diffusion equation:

287

$$288 \left(\frac{\partial C_{Fe/Mg}}{\partial t} \right)^\alpha = \frac{\partial}{\partial X} \left(D_{Fe-Mg}^\alpha \left(\frac{\partial C_{Fe/Mg}}{\partial X} \right)^\alpha \right) \quad (1)$$

289

290 using a finite difference scheme where α denotes the mineral phase. In this equation, the
291 actual change in concentrations of Fe and Mg ($C_{Fe/Mg}$) are calculated for each node (with node
292 spacing X) within the crystal for a given time interval t and the effective diffusion coefficient
293 D_{Fe-Mg} that is re-calculated after every time step according to the current temperature. Based
294 on the results by Mueller et al. (2013), an efficient adjustment of mineral compositions in both
295 phases above 1000 °C was assumed leading to initially flat concentration profiles.
296 Temperature dependent diffusion coefficients are calculated using the experimental data for
297 Fe-Mg interdiffusion in garnet (Borinski et al., 2012) and clinopyroxene (Mueller et al.,
298 2013). Fe and Mg concentrations for both phases at the interface are set to be in local
299 equilibrium, i.e. these concentrations followed a pressure and temperature dependent
300 partitioning:

301

302
$$K_D^{grt-cpx} = \frac{\left(\frac{Fe}{Mg}\right)^{grt}}{\left(\frac{Fe}{Mg}\right)^{cpx}} = f(P, T) \quad (2)$$

303

304 For this study, we used the partition coefficient derived by Ganguly et al. (1996). It is
305 important to bear in mind that the subtle differences in the transport properties of Fe and Mg
306 in clinopyroxene and garnet require an additional constraint to calculate the element fluxes
307 correctly. This becomes especially important in the case of simulated lamellae growth.
308 Consequently, mass balance is maintained for fluxes across the interface by:

309

310
$$D_{Fe-Mg}^{grt} \left(\frac{\partial C_{Fe/Mg}}{\partial X} \right)^{grt} = D_{Fe-Mg}^{cpx} \left(\frac{\partial C_{Fe/Mg}}{\partial X} \right)^{cpx} \quad (3)$$

311

312 Diffusion and partition coefficients are updated to the pressure and temperature corresponding
313 to the conditions attained at the time along a predefined exhumation and cooling path.
314 Resulting concentration profiles are calculated iteratively and final, frozen compositional
315 profiles are presented ranging from the center of the garnet lamella over the interface to the
316 center of the clinopyroxene lamella.

317 In the following, we explore three different model scenarios in order to separate and
318 evaluate the effects of cooling, exhumation and lamellae growth on the resulting recorded
319 chemical profile and compare the model results with the measured X_{Fe} distribution in the
320 natural sample. Final half-lamella dimensions of 80 μm for the garnet and 150 μm for the
321 clinopyroxene have been chosen to allow direct comparison of model results and natural
322 samples. The initial concentration in the garnet lamella has arbitrarily been set to $X_{Fe}=0.21$
323 and the corresponding clinopyroxene composition has been calculated to be in equilibrium
324 with the garnet at the P-T-conditions at the start of the model run using equation 2. For

325 simplicity, we selected a simple linear cooling and exhumation path for model runs with a
326 total duration of 2×10^3 , 2×10^4 , and 2×10^5 years, which corresponds to cooling rates of 2×10^5 ,
327 2×10^4 , and $2000 \text{ }^\circ\text{C}/\text{Ma}$, respectively.

328

329 *Case 1 – isobaric cooling / no lamellae growth*

330 A first set of models evaluate the effect of cooling on the compositional profiles
331 recorded in both the garnet and the clinopyroxene lamellae. Based on the results of Mueller et
332 al. (2013) which suggested complete (instantaneous) adjustment of compositions above 1000-
333 $1100 \text{ }^\circ\text{C}$ and an apparent closure between 600 and $700 \text{ }^\circ\text{C}$, we modeled a linear cooling from
334 1000 to $600 \text{ }^\circ\text{C}$ with different cooling rates. The pressure was chosen to 0.2 GPa which
335 corresponds to the final depth of emplacement of the massif. Our initial garnet composition of
336 $X_{\text{Fe}}=0.21$ results in an initial X_{Fe} of 0.1 in the clinopyroxene. We note that these values closely
337 correspond to the measured core compositions of both lamellae.

338 Modeling results for the case 1 scenario are shown in figure 4 (case 1). The recorded
339 profiles reveal a general increase in Fe in the garnet coupled to decrease of X_{Fe} in the
340 clinopyroxene, which is in agreement with the partition coefficient reflecting that Fe is more
341 compatible in garnet than in clinopyroxene with decreasing temperatures. Remarkably, both
342 lamellae exhibit a different Fe-zoning pattern with a slight increase from the center of the
343 garnet lamella towards the interface and a steep decrease of Fe concentration in clinopyroxene
344 towards the interface. The observed difference for the zoning pattern is the consequence of
345 two factors: (1) the smaller size of the garnet lamella results in a more efficient
346 homogenization. In addition, there is a Fe influx from the opposite grt-cpx interface which is
347 further promoted by (2) the higher diffusivity of Fe-Mg in garnet compared to clinopyroxene.
348 The slower transport of Fe and Mg through the clinopyroxene lattice causes an apparent
349 “depletion” of Fe near the interface. In other words, the limited supply of Fe from the lamella
350 interior produces a Fe-concentration gradient towards the interface. Sluggish diffusion within

13

351 the clinopyroxene also results in the preservation of the initial concentration for cooling
352 histories below 2×10^4 years, i.e. cooling rates above 2×10^4 °C/Ma. In addition, we noted that
353 the original clinopyroxene composition is completely reset at slower cooling rates. In contrast,
354 the smaller lamella size combined with faster diffusion erases the original garnet composition
355 for all cooling histories lasting longer than $\sim 10,000$ years, i.e. only extremely high cooling
356 rates of $> 4 \times 10^4$ °C/Ma, typical of contact metamorphism, will preserve the initial element
357 distribution in the center of the garnet lamella.

358 Comparison of the measured concentrations reveal that very short cooling histories
359 with very high cooling rates are necessary to produce modeled element distributions that are
360 in agreement with the observed ones. Slower cooling rates allowing more diffusive exchange
361 inevitably result in a stronger Fe-zoning in the clinopyroxene lamella which is not observed in
362 the natural sample. In the case of garnet, the model predicts the zoning profile, but much
363 higher Fe-concentrations would be expected.

364

365 *Case 2 – polybaric cooling / no lamellae growth*

366 In the second set of models we have explored the modification of the preserved
367 cooling profile due to the different temporal evolution of the partition coefficient if
368 exhumation, i.e. changes in the confining pressure, is taken into account. In theory, diffusive
369 migration of elements through the crystal lattice is also affected by changes in pressure, but to
370 our knowledge, no pressure dependent Fe-Mg interdiffusion data exist for clinopyroxene and
371 garnet. However, in most cases this pressure effect on diffusion becomes only significant at
372 very high pressures (Watson and Baxter, 2007; Mueller et al., 2010). Thus, we neglect a
373 possible minor pressure dependence of Fe-Mg interdiffusion for the purpose of this study.
374 Modeling results of this scenario are shown in figure 4 (case 2).

375 For the same initial garnet composition ($X_{\text{Fe}} = 0.21$) a starting composition for the
376 clinopyroxene of $X_{\text{Fe}} = 0.09$ results, which is slightly below the measured natural

377 concentration. We applied the same thermal histories as in case 1. The modeling results
378 exhibit similar features, i.e. formation of zoning patterns in both lamellae and a comparable
379 extent of increasing X_{Fe} in garnet countered by a decrease of X_{Fe} in clinopyroxene.
380 Nevertheless, subtle differences can be observed in both lamellae that are a direct
381 consequence of the partition coefficient being a function of pressure and temperature. Here,
382 decreasing pressure favors Fe incorporation into pyroxene, whereas decreasing temperatures
383 act in the opposite direction. As a consequence, the effective influx of iron into the garnet is
384 somewhat smaller which reduces the total increase in Fe-content. Nevertheless, cooling
385 timescales greater than 10^4 years for the cooling from 1000 °C to 600 °C modify the entire
386 initial lamellae compositions and produce a slight zoning pattern with increasing X_{Fe} towards
387 the interface. For the clinopyroxene, the model predicts an extended depletion of Fe near the
388 interface even for a short period of time of 2,000 years, but the initial composition is still
389 preserved in the center for cooling histories shorter than 10^5 years. Longer cooling times yield
390 flatter Fe-zoning compared to the case 1 scenario. In addition, the zoning significantly extends
391 into the lamella interior, which is in clear disagreement with the measured data.

392

393 *Case 3 – isobaric cooling / lamellae growth*

394 The effect of lamella growth on the developing concentration profile is the focus of the
395 third set of models. Given the minor impact of pressure changes on the recorded profiles in
396 case 2 scenarios and to separate each parameter, we decided to run this set of models at a
397 constant pressure of 0.2 GPa. Thus, all model parameters are the same as in case 1 models.
398 The garnet lamella with an initial thickness of 40 μm (cpx = 190 μm) grows linearly with time
399 by 40 μm to a final thickness of 80 μm over the duration of the calculation. The same amount
400 of clinopyroxene was consumed, ignoring any volume change induced by this reaction. Figure
401 4 (case 3) shows the modeling results for the case of isobaric cooling from 1000 °C to 600 °C
402 accompanied by the final growth stage of the garnet lamella at the expense of clinopyroxene.

403 The calculated final concentration profiles are generally similar to all previous model
404 scenarios. Again, spatial variations in the zoning pattern and differences in total Fe-content of
405 garnet can be observed. In the present case, the original garnet lamella composition is
406 completely modified even for short run durations of only 2,000 years. This is a direct
407 consequence of the small initial lamella size, which allows diffusion to efficiently transport Fe
408 to the center of the lamella. Interestingly, the model predicts only a very narrow Fe-zoning in
409 clinopyroxene near the interface. The reason for this is that the growing garnet basically
410 “consumes” the developing depletion in the clinopyroxene lamella progressively. Retention of
411 the original clinopyroxene composition in the center of the lamella corresponds exactly to the
412 case 1 models, i.e. preservation for thermal histories with cooling rates above 2×10^4 °C/Ma.

413

414 **Discussion**

415 The crystallization history of co-existing mineral phases is typically recorded in their
416 chemical compositions, the basic concept of geothermobarometry. Many metamorphic studies
417 have applied this concept to decipher the P-T evolution of a metamorphic rock and placed the
418 results into a larger geodynamic context. For example, a number of studies reconstructed P-T-
419 paths for rocks from the Bohemian Massif, particularly for those of higher metamorphic
420 grade. Such rocks occur in the Granulitgebirge (e.g., Roetzler and Romer, 2001; Massonne
421 and Bartsch, 2002; Roetzler et al., 2004; Roetzler et al., 2008; Schmaedicke et al., 2010).
422 While there is a general agreement over a clockwise P-T-path, it is often based on exchange
423 reactions applied to mineral pairs which are subject to retrograde, diffusive modification. In
424 addition, information on the timescales of geodynamic processes is mostly restricted to
425 geochronological data obtained on different minerals. To both ends, kinetic modeling allows
426 the placing of time constraints and evaluates if a mineral composition is reset and if so, to
427 what extent. In the following sections, we consider both equilibrium phase petrology and

428 kinetic modeling to determine timescales of different stages in the P-T evolution of rocks
429 from the Granulitgebirge in Saxony and compare our findings with previous studies.

430

431 *Reconstruction of the P-T-t path*

432 Decompression during exhumation, cooling and net mass transfer reactions are
433 recorded in the concentration profiles of the studied garnet and clinopyroxene lamellae
434 exsolved from a former megacryst. Mueller et al. (2013) presented convincing evidence that
435 mineral compositions rapidly adjust at temperatures above 1000 °C for most geological
436 settings. Therefore, modeling of the element distribution in the studied lamellae will only give
437 information on the thermal history below this temperature. The predicted profiles of all model
438 scenarios clearly suggest that cooling from 900-1000 °C was very fast (\ll 10,000 years)
439 indicated by the absence of pronounced zoning patterns, which are predicted for slower
440 cooling rates (Fig. 4). This short period of time, which is typical for contact metamorphic
441 aureoles such as that around the Adamello Batholith (Berger and Herwegh, 2004), and
442 Ubehebe Peak (Roselle et al., 1999; Mueller et al., 2008), is the first key observation that
443 result from the diffusion modeling presented here.

444 The first model of isobaric cooling at shallow crustal levels (mimicking simple contact
445 metamorphism) produced concentration profiles that do not exactly match the observed,
446 measured profiles (Fig. 4 – case 1). On the one hand, the concentration in the center of the
447 clinopyroxene lamella is in agreement with the measured data and represents the original
448 composition. On the other hand, the central garnet composition increased slightly, but not
449 sufficiently to exactly match the observed data for the 2,000 year cooling episode.
450 Surprisingly, the addition of continuously changing pressure conditions during cooling to
451 account for the exhumation of the massif does not improve the fittings (Fig. 4 – case 2). In
452 this case, the short time scales necessary to limit the spatial extent of the zoning patterns will
453 also preserve the initial clinopyroxene lamella composition in the center. Using the pressure

454 and temperature dependent partition coefficient we calculated an initial Fe-content which is
455 slightly below the observed data. As this calculation is a direct consequence of the arbitrarily
456 defined starting composition in garnet, this difference could be minimized by an increase of
457 the Fe-content in initial garnet. However, the pressure effect on the partition coefficient leads
458 to a flatter and broader zoning pattern in the clinopyroxene lamella in apparent contrast to the
459 measured profile (Fig. 4 – case 2). Hence, we interpret the apparent deviation of the predicted
460 profiles as an indication that the vast majority of the cooling history below 1000 °C took place
461 at or near the final depth of emplacement, i.e. at a pressure of about 0.2 GPa.

462 The effect of lamella growth on the final profiles is not substantial, but is discernable
463 in the final shape of the zoning pattern (Fig. 4 – case 3). Based on thermodynamic constraints
464 we assume that the garnet lamella grew about 50 % of its final size during cooling. The garnet
465 growth, in turn, results in a more efficient homogenization of the garnet leading to an increase
466 in the Fe-content up to the center of the lamella, which is in perfect agreement with the
467 measured data. At the same time, the progressive growth of garnet will consume the depletion
468 of Fe in clinopyroxene, resulting in a very narrow and steep zoning profile (Fig. 4 – case 3).
469 In conclusion of the diffusion modeling we interpret the observed Fe-Mg profiles in adjacent
470 grt-cpx lamellae to be the result of isobaric cooling from at least 900 – 600 °C within ~10,000
471 years at shallow crustal levels (~6 km depth).

472 The high cooling rates ($> 2 \times 10^5$ °C/Ma) predicted by the diffusion modeling are
473 common for contact aureoles as mentioned above. The presence of the schist mantle
474 surrounding the tectonically separated granulite complex of the Granulitgebirge (Fig. 1c) is
475 the consequence of contact metamorphism during the emplacement (Roetzler and Romer,
476 2010), which is in agreement with increasing metamorphic grade towards the tectonic contact
477 and has already been suggested by Frech (1917). The spatial extent of the contact
478 metamorphic halo in the schist mantle provides an excellent opportunity to independently
479 constrain the temperature of the Massif during emplacement of the granulite complex with a

480 simple thermal model. To that end, we modeled the T-t evolution of the granulite complex
481 and surrounding country rocks. The model assumes a tabular shape of the granulite complex
482 with a radius of 10 km. Figure 5 presents the temporal evolution of the thermal history in
483 rocks surrounding the Massif. Metamorphic temperatures necessary to form the exposed
484 phyllite from pelitic sediments are around 350 °C. Reported migmatites near the tectonic
485 contact require temperatures near 700 °C. Inspection of figure 5 reveals a maximum
486 dimension of about 1-3 km for the contact aureole in the western part. The spatial extension in
487 the eastern area is less, but this may be a cut effect of the current topography or the exact 3-D
488 position of the granulite complex. In addition, we monitor the cooling history of a rock
489 located about 1 km away from the contact within the granulite complex. This position is
490 approximately the location of the investigated lamellar garnet pyroxenite. Calculated thermal
491 histories are shown in figure 5. It can be seen that both, the spatial extent of the predicted
492 contact-metamorphic halo (Fig. 5) and cooling rates corresponding to those determined by the
493 diffusion modeling (Fig. 5 - inset), can well be estimated with this simplified thermal model
494 for a contact aureole assuming an initial temperature of ≥ 950 °C for the granulite complex. A
495 more detailed and sophisticated thermal model would be necessary to really constrain exact
496 initial temperatures, which is beyond the scope of this study. We note, however, that a
497 simplified thermal model is an independent second line of arguments supporting the results of
498 our diffusion modeling, i.e. the major cooling history that took place at almost isobaric
499 conditions after emplacement.

500 One major goal of this study is to place time constraints on different stages of the P-T-t
501 path. The heat and diffusion modeling provided two solid constraints. First, the major portion
502 of the cooling history from ~ 1000 -600 °C took place at almost isobaric conditions and
503 secondly this cooling episode occurred at a short timescale of several thousand years only.
504 Thus, the exhumation of the granulite complex is likely to follow an almost isothermal
505 decompression path (Fig. 6). Several studies have estimated the peak P-T conditions for most

506 rocks from the granulite complex to be around 2.2-2.3 GPa and $\geq 1000^\circ\text{C}$ (Roetzler and
507 Romer, 2001; Massonne and Bartsch, 2002; Roetzler et al., 2004; Roetzler et al., 2008;
508 Schmaedicke et al., 2010) ignoring the higher temperatures for the magmatic formation of the
509 megacrysts preceding the garnet pyroxenite from Reinsdorf. It is important to keep in mind
510 that determination of the above P-T conditions are based on geothermobarometry using the
511 core compositions of co-existing mineral pairs (e.g. grt-cpx). The modeling results of the
512 diffusive element exchange during cooling indicate that in the present case only the central
513 clinopyroxene composition remained unchanged. The garnet composition, in contrast, was
514 completely reset during cooling as a consequence of the smaller lamella size and faster
515 diffusion. Under these circumstances, conventional thermometry using core-core
516 compositions of co-existing mineral phases will either overestimate the pressure or
517 underestimate the temperature if the P-T dependent partition coefficient of Ganguly et al.
518 (1996) is applied. However, the results generally suggest a very limited cooling during the
519 exhumation process. While the exact reaction history remains unclear as discussed above, the
520 presence of a nearly isothermal decompression path sets some thermal constraints on the
521 timescale of exhumation. To that end, one can again use a very simplified thermal model to
522 evaluate the minimum exhumation rate for a block that cooled progressively inwards during
523 exhumation due to the decreasing temperature of the surrounding rocks within an
524 “exhumation channel”. Figure 7 shows the predicted temperature distribution after 1, 3 and 7
525 Ma for the block with the same geometry and heat transport properties as in the previous
526 calculation. In this model the contact temperature decreases linearly from 1200°C
527 representing the original root zone to 350°C mimicking the temperature of the sediments at
528 the final depth of emplacement at 0.2 GPa. It is important to keep in mind that the results of
529 the diffusive element exchange as well as the modeling of the thermal history of the aureole
530 revealed a minimum temperature of 900°C for the garnet-pyroxenite sample located about 1
531 km away from the contact. The simplified thermal model for the exhumation event of the

532 granulite complex suggests a maximum integrated time of exhumation to be less than 1 Ma,
533 which translates into an average exhumation rate of 4-5 cm/year. Slower exhumation rates are
534 likely to cool the outermost kilometer of the granulite complex to temperatures significantly
535 below 900 °C which is incompatible with the finding of the diffusion model. We note, that our
536 model has many simplifying assumptions, e.g. that there is no friction, latent heat of
537 crystallization, etc., and thus the extracted exhumation rates could be somewhat
538 overestimated. Again, we emphasize that a much more detailed thermal model is required to
539 constrain exact information of the thermal evolution of the granulite complex during
540 exhumation and cooling in order to verify our conclusions. However, our simple thermal
541 model calculations provide at least rough, but independent estimates which all point to the
542 same P-T-t evolution of the studied sample.

543

544 *Comparison with previous P-T-t estimates*

545 We combined our modeling results to construct a P-T-t path presented as path A in
546 figure 6. For comparison we added the reported P-T evolution of Roetzler and Romer (2001),
547 Roetzler et al. (2004, 2008) Schmaedicke et al. (2010), Massonne and Bartsch (2002),
548 Massonne (2006), and O'Brien (2008). The latter author studied the P-T path of co-existing
549 garnet and clinopyroxene in rocks from the southern Bohemian Massif which belongs to the
550 same overall geological setting, but has a different final depth of emplacement (0.8 GPa). The
551 P-T-path of Roetzler and Romer (2001), and Roetzler et al. (2004, 2008) derived by a series of
552 studies summarized in Roetzler and Romer (2010) and the geological settings of the current
553 study, is based on conventional thermobarometry and multivariant reactions (path C in figure
554 6). For example, peak P-T conditions are estimated on felsic and mafic granulite using the Fe-
555 Mg exchange thermometry between co-existing garnet and clinopyroxene, re-integrated
556 feldspar composition and equilibrium oxygen isotope fractionations. All approaches,
557 including the geothermobarometry data of Massonne and Bartsch (2002) and Schmaedicke

558 (2010), yield a very narrow range of apparent peak temperatures around 1000 °C. However, in
559 the light of this study it could be that this coincidence is an artefact of efficient element and
560 isotope exchange leading to an effective preservation of the compositional record at
561 temperatures below 1000 °C. This is certainly true for element and isotope exchange
562 processes which are kinetically controlled, i.e. Fe-Mg exchange and oxygen isotope
563 thermometry. Re-integration of feldspar composition might give more robust information.
564 Roetzler & Romer (2001) and Roetzler et al. (2004, 2008) applied the commonly used GASP
565 barometer to estimate the peak pressure conditions. Again, caution is necessary when
566 applying this barometer using the possibly modified garnet composition. To account for this
567 we expanded the P-T pressure range extracted by Roetzler and Romer (2001), Roetzler et al.
568 (2004, 2008), Massonne and Bartsch (2002) and Schmaedicke (2010) to include lower and
569 higher temperatures.

570 P-T estimates for the garnet-cordierite-gneiss were used as a second constraint for the
571 P-T-path by Romer and Rötzler (2010) who proposed a decompression-heating path for the
572 rocks that have been incorporated into the ascending granulite complex. Several models exist
573 for the exhumation mechanism of the Variscan HP-HT rocks (Franke and Stein, 2000;
574 Willner et al., 2002; Massonne, 2006; Kroner et al., 2007). For the purpose of this study it is
575 not necessary to discriminate between the many existing models as only the time response of
576 mineral compositions on the exhumation process is considered here. A schematic model for
577 the ascent of the granulite core in an “exhumation channel” (Fig. 8) illustrates the
578 consequences of the P-T conditions determined for the garnet-cordierite gneiss (Fig. 8) on the
579 P-T-t path of the studied garnet-pyroxenite sample. There is general agreement that the
580 garnet-cordierite gneiss became attached on the granulite complex during exhumation. During
581 this uptake, this rock was heated by the rising granulite complex which is documented by the
582 decompression-heating path proposed by Romer and Roetzler (2001). These authors
583 concluded that the granulite complex had the same temperature as the surrounding gneiss

584 which is represented by the cooling path in figure 6 (path C3 and C). Again, transport of heat
585 is not instantaneous and thus the heating of the uptaken rock portion can be imagined as a
586 contact metamorphic event along the short-lived exhumation process. In other words, while
587 there is no doubt that the metamorphic garnet-cordierite gneiss experienced the proposed
588 decompression-heating path, there is no direct evidence of similar low temperatures for the
589 central part of the granulite complex. In contrast, sluggish heat transfer is likely to decouple
590 the thermal history for the different lithologies leaving the thermal evolution of the original
591 block near its isothermal behavior due to adiabatic cooling only in agreement with our
592 modeling results (Fig. 8).

593 In a recent study, Schmaedicke et al. (2010) presented a series of thermometric data of
594 the garnet peridotites and garnet pyroxenites exhibiting kelyphitic reaction textures
595 surrounding garnet crystals of the same locality. Thermometry data based on Fe-Mg exchange
596 revealed the same P-T estimates for grt-cpx and grt-olivine pairs (~2.4 GPa, ~1000 °C).
597 However, co-existing opx-cpx pairs in the kelyphitic reaction rims yield systematically lower
598 temperatures ranging from 890-940 °C for the garnet peridotite (at 2.0 GPa) and 840 °C at 1.5
599 GPa for the garnet pyroxenite, respectively. We note that the symplectites observed in our
600 sample replacing garnet have to be formed after the formation of the grt-cpx lamellae, i.e.
601 after exhumation to approximately 0.2 GPa. However, the lower temperature estimates have
602 led Schmaedicke (2010) to shift the reconstructed P-T-path to be located around 100 °C
603 lower, but parallel to previous estimates (path E in Fig. 6). This interpretation favors the opx-
604 cpx data and neglects the results of the grt-cpx and feldspar thermometry. In the light of our
605 modeling results, however, it is likely that the opx-cpx pairs have experienced a more efficient
606 element exchange, which results in a larger reset of the preserved, i.e. measured temperatures.
607 While the diffusion coefficients of Fe-Mg interdiffusion in grt and opx are similar at the
608 relevant temperature range (Mueller et al., 2013), this interpretation is supported by the
609 mostly pressure sensitive, continuous reaction forming the opx-cpx-spinel kelyphite texture at

610 pressures below 2.0 GPa. Modeling results of our case 3 scenarios revealed that mineral
611 growth leads to more efficient homogenization and thus the progressive cooling would be
612 preferentially recorded in cpx-opx pairs while already existing grt-cpx pairs experience more
613 sluggish adjustment of central compositions. Hence, we attribute the lower temperatures
614 extracted by opx-cpx thermometry in kelyphitic reaction rims to diffusive closure of element
615 exchange at lower temperatures and thus at a later stage during cooling on the retrograde path.
616 Excluding the opx-cpx thermometric data in the study of Schmaedicke et al. (2010) would
617 shift the resulting P-T path towards higher temperatures and thus perfectly fit the data of
618 Roetzler and Romer (2008).

619 In a very thorough study of rocks from the southwestern part of the Bohemian Massif,
620 O'Brien (2008) presented convincing evidence for a very similar isothermal decompression
621 path around 1000 °C using thermodynamic phase equilibria calculations on whole rock
622 chemistry and element zoning in grt-cpx pairs (path G in figure 6). In this case, the isothermal
623 exhumation is followed by an almost isobaric cooling episode at approximately 0.8 GPa.
624 Here, the metamorphic block is supposed to have not been exhumed to the same extent as in
625 the granulite complex. Given the greater depth of emplacement, the reconstructed P-T
626 evolution of O'Brien (2008) is in good agreement with our findings. We thus interpret all of
627 these rocks to have been exhumed by the same, although unknown mechanism and most
628 likely the same rates, but to different final depths. This interpretation highlights the potential
629 of combining equilibrium phase petrology with kinetic modeling to decipher rates and
630 mechanisms of large-scale geodynamic processes.

631

632 **Implications**

633 We applied kinetic modeling to decipher the effect of changing external parameters,
634 i.e. pressure and temperature, on the evolution of concentration profiles in minerals which are
635 direct recorders of geochemical fluxes in metamorphic rocks. The fact, that minerals adjust

636 their compositions according to external parameters, is typically used to reconstruct the P-T-
637 evolution of a rock using a combination of available geothermobarometers. In this study, we
638 demonstrate that care has to be taken by using geothermobarometric data to reconstruct P-T-
639 paths without constraining the kinetically controlled efficiency of geochemical fluxes. While
640 there is no doubt that geochemical exchange records the change of external temperatures and
641 pressures, it often remains the question by how much. In other words, the temperatures
642 determined by rim-rim and core-core compositions may not necessarily reflect peak
643 metamorphic or any other assigned conditions as previously suggested by Dohmen and
644 Chakraborty (2003) and Faryad and Chakraborty (2005). Additional information is necessary
645 to place these data into a larger context within a petrogenetic grid. Modeling of the diffusive
646 element exchange during cooling provides a solid estimate for the extent of reset allowing the
647 temperature data to be interpreted as dynamically evolving parameter. Moreover, this study
648 highlights the potential of assigning timescales not only to geological settings with large P-T
649 changes over short time-intervals such as contact aureoles, but also on large scale
650 geodynamical processes in regional metamorphic settings.

651 The diffusive exchange model was used to extract the major cooling episode at
652 shallow crustal levels which is in agreement with the thermal modeling that requires the
653 emplacement of the granulite block at temperatures above 900 °C in order to produce the
654 observed contact metamorphism in the schist mantle and the phyllite zone. This in turn
655 requires an almost isothermal exhumation from great depth at rates comparable to active plate
656 movements of several cm per year. While modeling of the mineral zoning in grt-cpx pairs
657 places narrow limits on the timescales of the final cooling episode, the evaluation of
658 timescales for the exhumation is much more complex. Our very simplified thermal model for
659 the exhumation process only suggests a very rapid exhumation and consequently has to be
660 regarded as an end-member model. The other extreme would be a slow adiabatic exhumation
661 in which case no time-related information is recorded. Hence, much more detailed thermal

662 modeling within the context of geodynamical transport processes is necessary to extract more
663 detailed information on the exhumation rate of the Granulitgebirge. We close this section by
664 emphasizing that every conceptual model explaining a large scale exhumation process needs
665 to fit the geochemical record preserved in the spatial element distribution within minerals.

666

667 **Acknowledgments**

668 This study was financially supported by grants from the Ruhr-University Bochum to
669 T. Mueller partly covering the travel expenses for this collaboration. The ideas and models
670 presented here benefited greatly from discussion with Sumit Chakraborty in the course of
671 developing the numerical model. We thank Thomas Theye for the help with the electron
672 microprobe analysis. We greatly acknowledge the constructive reviews of C. Tom Foster and
673 Ryszard Kryza as well as comments and the editorial handling by John Ferry.

674

675 **References**

- 676 Berger, A., and Herwegh, M. (2004) Grain coarsening in contact metamorphic carbonates:
677 effects of second-phase particles, fluid flow and thermal perturbations. *Journal of*
678 *Metamorphic Geology*, 22(5), 459-474.
- 679 Borinski, S.A., Hoppe, U., Chakraborty, S., Ganguly, J., and Bhowmik, S.K. (2012)
680 Multicomponent diffusion in garnets I: general theoretical considerations and
681 experimental data for Fe-Mg systems. *Contributions to Mineralogy and Petrology*,
682 164(4), 571-586.
- 683 Caddick, M.J., Konopásek, J., and Thompson, A.B. (2010) Preservation of garnet growth
684 zoning and the duration of prograde metamorphism. *Journal of Petrology*, 51(11),
685 2327-2347.
- 686 Costa, F., Dohmen, R., and Chakraborty, S. (2008) Time Scales of Magmatic Processes from
687 Modeling the Zoning Patterns of Crystals. *Minerals, Inclusions and Volcanic*
688 *Processes*, 69, 545-594.
- 689 Cruz-Uribe, A.M., Feineman, M.D., Zack, T., and Barth, M. (2014) Metamorphic reaction
690 rates at ~650–800° C from diffusion of niobium in rutile. *Geochimica Et*
691 *Cosmochimica Acta*, 130, 63-77.

- 692 Dodson, M.H. (1973) Closure temperature in cooling geochronological and petrological
693 systems. *Contributions to Mineralogy and Petrology*, 40(3), 259-274.
- 694 -. (1986) Closure profiles in cooling systems. *Materials Science Forum*, 7, p. 145-153. Trans
695 Tech Publications, Aedermannsdorf, Switzerland.
- 696 Dohmen, R., and Chakraborty, S. (2003) Mechanism and kinetics of element and isotopic
697 exchange mediated by a fluid phase. *American Mineralogist*, 88(8-9), 1251-1270.
- 698 Ducea, M.N., Ganguly, J., Rosenberg, E.J., Patchett, P.J., Cheng, W.J., and Isachsen, C.
699 (2003) Sm-Nd dating of spatially controlled domains of garnet single crystals: a new
700 method of high-temperature thermochronology. *Earth and Planetary Science Letters*,
701 213(1-2), 31-42.
- 702 Fisher, G.W. (1978) Rate laws in metamorphism. *Geochimica et Cosmochimica Acta*, 42,
703 1035-1050.
- 704 Franke, W., and Stein, E. (2000) Exhumation of high-grade rocks in the Saxo-Thuringian
705 Belt: geological constraints and geodynamic concepts. Geological Society, London,
706 Special Publications, 179(1), 337-354.
- 707 Frech, F. (1917) *Allgemeine Geologie I: Vulkane einst und jetzt*. Teubner Verlag, Leipzig.
- 708 Gaidies, F., De Capitani, C., Abart, R., and Schuster, R. (2008a) Prograde garnet growth
709 along complex P–T–t paths: results from numerical experiments on polyphase garnet
710 from the Wölz Complex (Austroalpine basement). *Contributions to Mineralogy and
711 Petrology*, 155(6), 673-688.
- 712 Gaidies, F., Krenn, E., De Capitani, C., and Abart, R. (2008b) Coupling forward modelling of
713 garnet growth with monazite geochronology: an application to the Rappold Complex
714 (Austroalpine crystalline basement). *Journal of Metamorphic Geology*, 26(7), 775-
715 793.

- 716 Gaidies, F., Pattison, D., and de Capitani, C. (2011) Toward a quantitative model of
717 metamorphic nucleation and growth. *Contributions to Mineralogy and Petrology*,
718 162(5), 975-993.
- 719 Ganguly, J., Cheng, W., and Tirone, M. (1996) Thermodynamics of aluminosilicate garnet
720 solid solution: new experimental data, an optimized model, and thermometric
721 applications. *Contributions to Mineralogy and Petrology*, 126(1-2), 137-151.
- 722 Ganguly, J., and Tazzoli, V. (1994) Fe²⁺-Mg interdiffusion in ortho-pyroxene - retrieval from
723 the data on intercrystalline exchange reaction. *American Mineralogist*, 79(9-10), 930-
724 937.
- 725 Ganguly, J., and Tirone, M. (1999) Diffusion closure temperature and age of a mineral with
726 arbitrary extent of diffusion: theoretical formulation and applications. *Earth and*
727 *Planetary Science Letters*, 170(1-2), 131-140.
- 728 Ganguly, J., Tirone, M., Chakraborty, S., and Domanik, K. (2013) H-chondrite parent
729 asteroid: A multistage cooling, fragmentation and re-accretion history constrained by
730 thermometric studies, diffusion kinetic modeling and geochronological data.
731 *Geochimica Et Cosmochimica Acta*, 105(0), 206-220.
- 732 Grew, E.S. (1986) Petrogenesis of kornerupine at Waldheim (Sachsen), German-Democratic-
733 Republic. *Zeitschrift fuer geologische Wissenschaften*, 14(5), 525-558.
- 734 Hagen, B., Hoernes, S., and Roetzler, J. (2008) Geothermometry of the ultrahigh-temperature
735 Saxon granulites revisited. Part II: Thermal peak conditions and cooling rates inferred
736 from oxygen-isotope fractionations. *European Journal of Mineralogy*, 20(6), 1117-
737 1133.
- 738 Hauzenberger, C.A., Robl, J., and Stuwe, K. (2005) Garnet zoning in high pressure granulite-
739 facies metapelites, Mozambique belt, SE-Kenya: constraints on the cooling history.
740 *European Journal of Mineralogy*, 17(1), 43-55.

- 741 Hentschel, H. (1937) Der Eklogit von Gilsberg im sächs. Granulitgebirge und seine
742 metamorphen Umwandlungsstufen. Zeitschrift für Kristallographie, Mineralogie und
743 Petrographie, 49(1), 42-88.
- 744 Jekosch, U., and Bautsch, H. (1991) Orientierte Entmischungen in Pyroxenen. Zeitschrift für
745 Kristallographie: Supplement (XIII European Crystallographic Meeting), 4, p. 134.
- 746 Kroener, A., Jaeckel, P., Reischmann, T., and Kroner, U. (1998) Further evidence for an early
747 Carboniferous (similar to 340 Ma) age of high-grade metamorphism in the Saxonian
748 granulite complex. Geologische Rundschau, 86(4), 751-766.
- 749 Kroener, A., and Willner, A.P. (1998) Time of formation and peak of Variscan HP-HT
750 metamorphism of quartz-feldspar rocks in the central Erzgebirge, Saxony, Germany.
751 Contributions to Mineralogy and Petrology, 132(1), 1-20.
- 752 Kroner, U., and Goerz, I. (2010) Variscan assembling of the Allochthonous Domain of the
753 Saxo-Thuringian Zone—a tectonic model. In U. Linnemann, and R.L. Romer, Eds. Pre-
754 Mesozoic Geology of Saxo-Thuringia—from the Cadomian Active Margin to the
755 Variscan Orogen. Schweizerbart, Stuttgart, p. 271-286. Schweizerbart, Stuttgart.
- 756 Kroner, U., Hahn, T., Romer, R.L., and Linnemann, U. (2007) The Variscan orogeny in the
757 Saxo-Thuringian zone-heterogenous overprint of Cadomian/Paleozoic Peri-Gondwana
758 crust. 153 p. Geological Society of America.
- 759 Kroner, U., and Romer, R.L. (2013) Two plates - Many subduction zones: The Variscan
760 orogeny reconsidered. Gondwana Research, 24(1), 298-329.
- 761 Lasaga, A.C. (1983) Geospeedometry: an extension of geothermometry. Kinetics and
762 equilibrium in mineral reactions, p. 81-114. Springer.
- 763 Lasaga, A.C., Richardson, S.M., and Holland, H.D. (1977) The mathematics of cation
764 diffusion and exchange between silicate minerals during retrograde metamorphism,. In
765 S.K. Saxena, and S. Bhattachanji, Eds. Energetics of Geological Processes, p. 353-
766 388. Springer-Verlag, New York.

- 767 Liermann, H.-P., and Ganguly, J. (2002) Diffusion kinetics of Fe²⁺ and Mg in aluminous
768 spinel: experimental determination and applications. *Geochimica Et Cosmochimica*
769 *Acta*, 66(16), 2903-2913.
- 770 Lucassen, F., Franz, G., Dulski, P., Romer, R., and Rhede, D. (2011) Element and Sr isotope
771 signatures of titanite as indicator of variable fluid composition in hydrated eclogite.
772 *Lithos*, 121(1), 12-24.
- 773 Massonne, H.-J. (2006) Early metamorphic evolution and exhumation of felsic high-pressure
774 granulites from the north-western Bohemian Massif. *Mineralogy and Petrology*, 86(3-
775 4), 177-202.
- 776 -. (2011) Occurrences and PT conditions of high and ultrahigh pressure rocks in the Bohemian
777 Massif. *Geolines*, 23, 18-26.
- 778 Massonne, H.-J., and Bartsch, H.J. (2002) An unusual garnet pyroxenite from the
779 Granulitgebirge, Germany: Origin in the transition zone (> 400 km depths) or in a
780 shallower upper mantle region? *International Geology Review*, 44(9), 779-796.
- 781 Massonne, H.-J., Kennedy, A., Nasdala, L., and Theye, T. (2007) Dating of zircon and
782 monazite from diamondiferous quartzofeldspathic rocks of the Saxonian Erzgebirge–
783 hints at burial and exhumation velocities. *Mineralogical Magazine*, 71(4), 407-425.
- 784 Massonne, H.-J., and O'Brien, P.J. (2003) The Bohemian massif and the NW Himalaya.
- 785 Mueller, T., Baumgartner, L.P., Foster, C.T., Jr., and Roselle, G.T. (2008) Forward modeling
786 of the effects of mixed volatile reaction, volume diffusion, and formation of
787 submicroscopic exsolution lamellae on calcite-dolomite thermometry. *American*
788 *Mineralogist*, 93(8-9), 1245-1259.
- 789 Mueller, T., Baumgartner, L.P., Foster, C.T., and Vennemann, T.W. (2004) Metastable
790 prograde mineral reactions in contact aureoles. *Geology*, 32(9), 821-824.
- 791 Mueller, T., Dohmen, R., Becker, H., ter Heege, J.H., and Chakraborty, S. (2013) Fe–Mg
792 interdiffusion rates in clinopyroxene: experimental data and implications for Fe–Mg

- 793 exchange geothermometers. *Contributions to Mineralogy and Petrology*, 166(6), 1563-
794 1576.
- 795 Mueller, T., Watson, E.B., and Harrison, T.M. (2010) Applications of Diffusion Data to High-
796 Temperature Earth Systems. *Reviews in Mineralogy and Geochemistry*, 72(1), 997-
797 1038.
- 798 O'Brien, P.J. (2008) Challenges in high-pressure granulite metamorphism in the era of
799 pseudosections: reaction textures, compositional zoning and tectonic interpretation
800 with examples from the Bohemian Massif. *Journal of Metamorphic Geology*, 26(2),
801 235-251.
- 802 Reiche, M., and Bartsch, H.-J. (1985) Electron microscopical study of garnet exsolution in
803 orthopyroxene. *Physics and Chemistry of Minerals*, 12(1), 29-33.
- 804 Reiche, M., and Bartsch, H. (1984) Entmischungsstrukturen in Pyroxenen aus eklogitischen
805 Gesteinen. *Freiberger Forschungshefte*, 393, 19-33.
- 806 Reinhardt, J., and Kleemann, U. (1994) Extensional unroofing of granulitic lower crust and
807 related low-pressure, high-temperature metamorphism in the Saxonian Granulite
808 Massif, Germany. *Tectonophysics*, 238(1-4), 71-94.
- 809 Roetzler, J., Hagen, B., and Hoernes, S. (2008) Geothermometry of the ultrahigh-temperature
810 Saxon granulites revisited. Part I: New evidence from key mineral assemblages and
811 reaction textures. *European Journal of Mineralogy*, 20(6), 1097-1115.
- 812 Roetzler, J., Kurze, M., Linnemann, U., and Troeger, K.-A. (1992) Zur Petrogenese im
813 sächsischen Granulitgebirge die pyroxenfreien Granulite und die Metapelite ; mit 12
814 Tab. = On the petrogenesis in the Saxon Granulite Massif. *Schweizbart, Stuttgart*.
- 815 Roetzler, J., and Romer, R. (2010) The Saxon Granulite Massif: a key area for the
816 geodynamic evolution of Variscan central Europe. *Pre-Mesozoic Geology of Saxo-
817 Thuringia—from the Cadomian Active Margin to the Variscan Orogen*. *Schweizerbart,
818 Stuttgart*, 233-252.

- 819 Roetzler, J., and Romer, R.L. (2001) P-T-t evolution of ultrahigh-temperature granulites from
820 the Saxon Granulite Massif, Germany. Part I: Petrology. *Journal of Petrology*, 42(11),
821 1995-2013.
- 822 Roetzler, J., Romer, R.L., Budzinski, H., and Oberhansli, R. (2004) Ultrahigh-temperature
823 high-pressure granulites from Tirschheim, Saxon Granulite Massif, Germany: P-T-t
824 path and geotectonic implications. *European Journal of Mineralogy*, 16(6), 917-937.
- 825 Romer, R.L., and Roetzler, J. (2001) P-T-t evolution of ultrahigh-temperature granulites from
826 the Saxon Granulite Massif, Germany. Part II: Geochronology. *Journal of Petrology*,
827 42(11), 2015-2032.
- 828 Roselle, G.T., Baumgartner, L.P., and Chapman, J.A. (1997) Nucleation-dominated
829 crystallization of forsterite in the Ubehebe Peak contact aureole, California. *Geology*,
830 25(9), 823-826.
- 831 Roselle, G.T., Baumgartner, L.P., and Valley, J.W. (1999) Stable isotope evidence of
832 heterogeneous fluid infiltration at the Ubehebe Peak contact aureole, Death Valley
833 National Park, California. *American Journal of Science*, 299(2), 93-138.
- 834 Schmaedicke, E., Gose, J., and Will, T.M. (2010) The P-T evolution of ultra high temperature
835 garnet-bearing ultramafic rocks from the Saxonian Granulitgebirge Core Complex,
836 Bohemian Massif. *Journal of Metamorphic Geology*, 28(5), 489-508.
- 837 Spear, F.S., and Florence, F.P. (1992) Thermobarometry in granulites - pitfalls and new
838 approaches. *Journal of Precambrian Research*, 55, 209-241.
- 839 Trepmann, C.A., Stockhert, B., and Chakraborty, S. (2004) Oligocene trondhjemitic dikes in
840 the Austroalpine basement of the Pfunderer Berge, Sudtirol - level of emplacement
841 and metamorphic overprint. *European Journal of Mineralogy*, 16(4), 641-659.
- 842 von Quadt, A. (1993) The Saxonian Granulite Massif - New aspects from geochronological
843 studies. *Geologische Rundschau*, 82(3), 516-530.

- 844 Watson, E.B., and Baxter, E.F. (2007) Diffusion in solid-Earth systems. *Earth and Planetary*
845 *Science Letters*, 253(3), 307-327.
- 846 Werner, C.D. (1987) Saxonian granulites: a contribution to the geochemical diagnosis of
847 original rocks in high-metamorphic complexes. *Gerlands Beiträge der Geophysik*, 96,
848 271-290.
- 849 Werner, O., and Reich, S. (1997) $^{40}\text{Ar}/^{39}\text{Ar}$ Abkühlalter von Gesteinen mit
850 unterschiedlicher PT-Entwicklung aus dem Schiefermantel des Sächsischen
851 Granulitgebirges. *Terra Nostra*, 97(5), 196-198.
- 852 Willner, A.P., Krohe, A., and Maresch, W.V. (2000) Interrelated P-T-t-d paths in the Variscan
853 Erzgebirge dome (Saxony, Germany): Constraints on the rapid exhumation of high-
854 pressure rocks from the root zone of a collisional orogen. *International Geology*
855 *Review*, 42(1), 64-85.
- 856 Willner, A.P., Sebazungu, E., Gerya, T.V., Maresch, W.V., and Krohe, A. (2002) Numerical
857 modelling of PT-paths related to rapid exhumation of high-pressure rocks from the
858 crustal root in the Variscan Erzgebirge Dome (Saxony/Germany). *Journal of*
859 *Geodynamics*, 33(3), 281-314.

860

861

862 **Figure captions**

863 **Figure 1:** (a) Location of the Granulitgebirge within the Variscan Bohemian Massif of
864 Central Europe with the distribution of high-pressure rocks (redrawn after Willner et al.,
865 2000). (b) Geological Map of the Granulitgebirge modified after Reinhardt and Kleemann
866 (1994) with the location of the garnet pyroxenite sample. (c) Simplified cross section of the
867 Granulitgebirge after Reinhardt and Kleemann (1994). Note that the black units shown in
868 panels (b) and (c) contain both, garnet peridotite and garnet pyroxenite.

869

870 **Figure 2:** Thin section image of garnet-pyroxenite sample under crossed polarized light. (A)
871 Image showing the dimensions of the former cm-sized megacryst within a matrix of
872 recrystallized garnet and clinopyroxene. (B) Alternating lamellae of garnet and clinopyroxene
873 with a final volume ratio of 3:7 are formed within the megacryst during exhumation and
874 cooling.

875

876 **Figure 3:** Representative compositional profiles of major and minor elements within adjacent
877 garnet and clinopyroxene lamellae measured with an electron microprobe. Line profiles reveal
878 almost flat, but weakly zoned patterns with increasing X_{Fe} from the garnet center towards the
879 interface. Almost no zoning for X_{Fe} can be observed in the cpx lamella. Minor elements show
880 an increase in concentration for Cr and Ti within the clinopyroxene towards the interface. In
881 contrast, no zoning is visible in the garnet. Note, that the garnet lamella is nearly free of Ti.

882

883 **Figure 4:** Modeling results using a finite difference scheme that simulates diffusive exchange
884 of Fe-Mg between garnet and clinopyroxene along a virtual cooling and exhumation path. The
885 model assumes local equilibrium at the interface and diffusive fluxes are constrained by mass
886 balance. Three different scenarios are modeled to investigate the effect of cooling (case 1),
887 exhumation (case 2) and growth (case 3) on the developing concentration profiles.
888 Progressively evolving concentration profiles are shown ranging from the initial step profile
889 up to 0.2 Ma. Note that only a combination of cooling on very short timescales of several
890 thousands of years in combination with growth of the garnet lamella is in agreement with the
891 measured data.

892

893 **Figure 5:** Thermal modeling of the contact metamorphic aureole producing the schist mantle
894 and the phyllite surrounding the granulite block. The numerical 1-D model assumes a tabular
895 shaped geometry of the granulite block and a general thermal diffusivity of $1 \times 10^{-6} \text{ m}^2/\text{s}$.

34

896 Temperature profiles are shown for different times ranging from 2k to 200k years. Note, that
897 temperatures necessary to match the spatial extent of the schist mantle and the surrounding
898 phyllite require an emplacement temperature of more than 900 °C for the granulite complex.
899 The black box represents the temperature estimates of the mantle schist as summarized in
900 Roetzler and Romer (2010). *Inset:* Modeled temperature-time path for the approximate
901 position of the garnet peridotite sample of this study as well as selected locations for rocks of
902 the mantle schist and the phyllite zone. Note that the major cooling episode (950-780 ° C) of
903 the garnet peridotite takes place in less than 2,000 years, which is in agreement with the short
904 modeled time scales for the Fe-Mg concentration profiles presented in figure 4.

905

906 **Figure 6:** Synopsis of modelled and determined P-T paths in the Granulitgebirge. A -
907 modelled P-T path of the granulite complex of this work; B - observed progressive contact
908 metamorphism in the schist mantle after Roetzler et al. (1992), Reinhardt and Kleemann
909 (1994) and Roetzler and Romer (2010); C - observed P-T-path of the granulite complex after
910 Roetzler & Romer (2001; 2010); C1 - observed peak conditions (Roetzler and Romer, 2001;
911 Roetzler et al. 2004, 2008; Hagen et al. 2008); C2 - symplectite stage (Roetzler et al. 2008);
912 C3- observed decompression-heating path of the garnet-cordierite gneiss (Rötzler & Romer
913 2010); D – observed late exhumation path of garnet pyroxenite after Massonne and Bausch
914 (2002); E - observed late exhumation path of garnet peridotite after Schmaedicke et al. (2010);
915 E1, 2- observed conditions of two symplectite stages (Schmaedicke et al., 2010); F - observed
916 local early stage metamorphic conditions (Massonne, 2006); G - observed P-T path of a high-
917 pressure granulite from the southwestern Bohemian Massif emplaced at mid-crustal
918 conditions (O'Brien, 2008).

919

920 **Figure 7:** Simplified numerical model simulating the cooling of the granulite block upon
921 exhumation in contact with an infinite reservoir of country rock with a linear geotherm. The

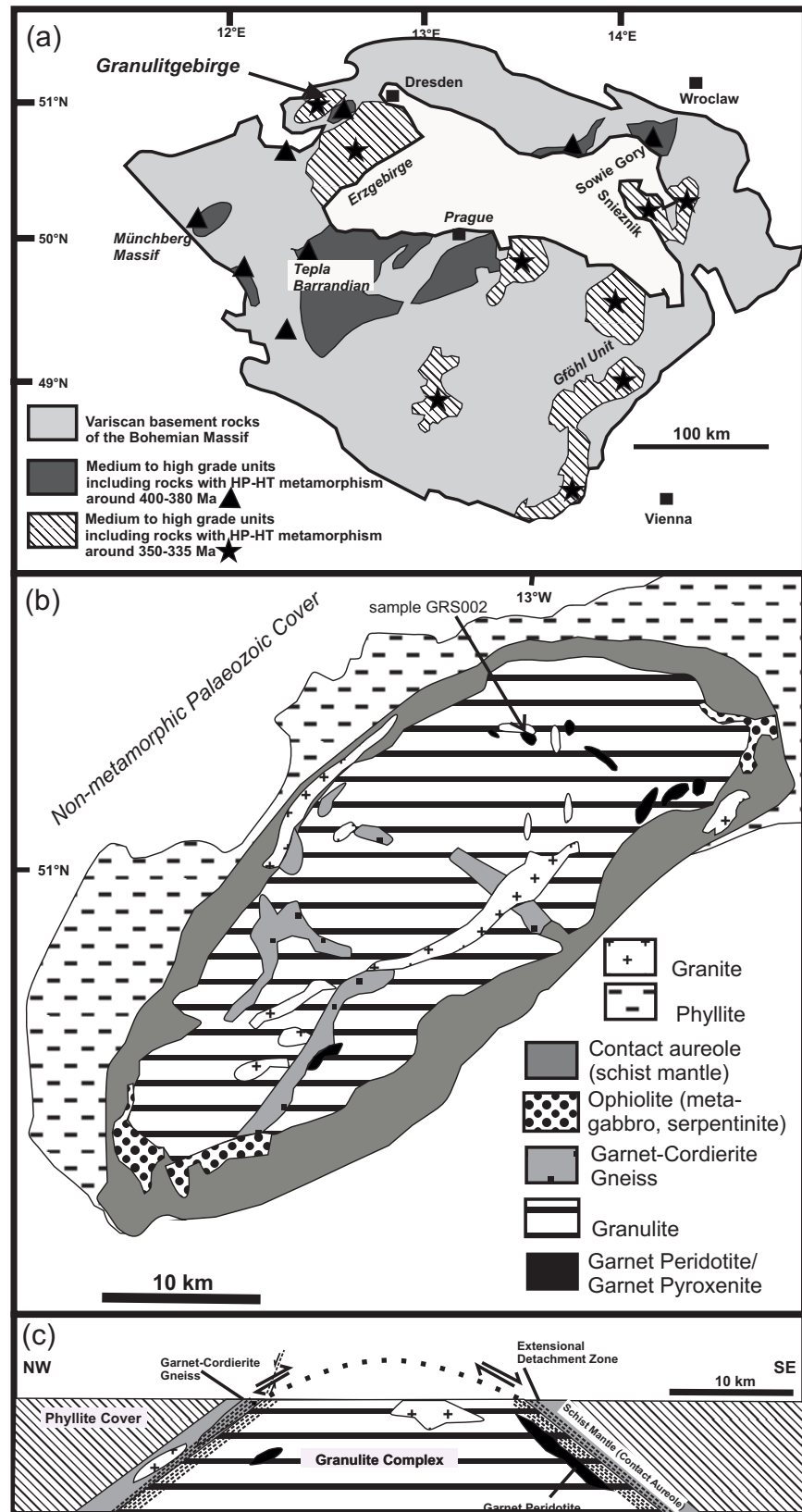
35

922 original temperature of the block and the surrounding was set to 1200 °C according to the
923 assumption of clinopyroxene as original host phase. The country rock is assumed to
924 geothermally equilibrate with depth forming a linear gradient that is opposed to the interface
925 of the exhumed tabular shaped block. Modeled thermal profiles are shown for exhumation
926 times ranging from 1-7 Ma. No external heat source (e.g. friction, latent heat of
927 crystallization, etc.) within an “exhumation channel” was taken into account by this simplified
928 model, which means that the determined timescales have to be regarded as minimum
929 timescales, i.e. maximum rates of exhumation. Nevertheless, the results emphasize the fast
930 exhumation rates in the order of several cm per year are necessary to preserve temperatures
931 higher than 900 °C. Such temperatures are required to match the spatial dimensions of the
932 formed contact aureole.

933

934 **Figure 8:** Mechanistic model explaining the observed temperature-time evolution of three
935 rock units between A - the position before the ascent of the granulite complex in extensional
936 detachment zones within an “exhumation channel” (a), i.e. during concomitant convergence -
937 and B - after emplacement of the granulite complex within the schist mantle at shallow crustal
938 conditions. Temperature-time evolution of (b) the schist mantle near the contact to the
939 granulite complex, (c) the mid-crustal garnet-cordierite gneiss emplaced during coupled
940 motion at the contact, (d) the granulite complex.

941



Mueller et al.
 Figure 1

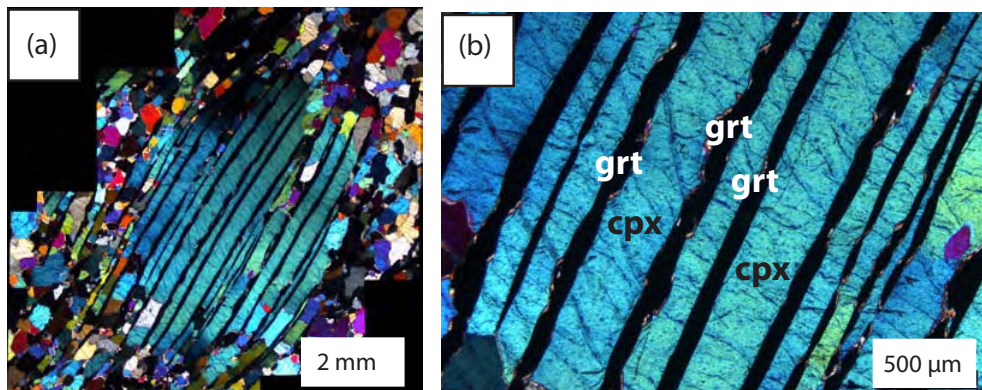


Figure 2
Müller et al.

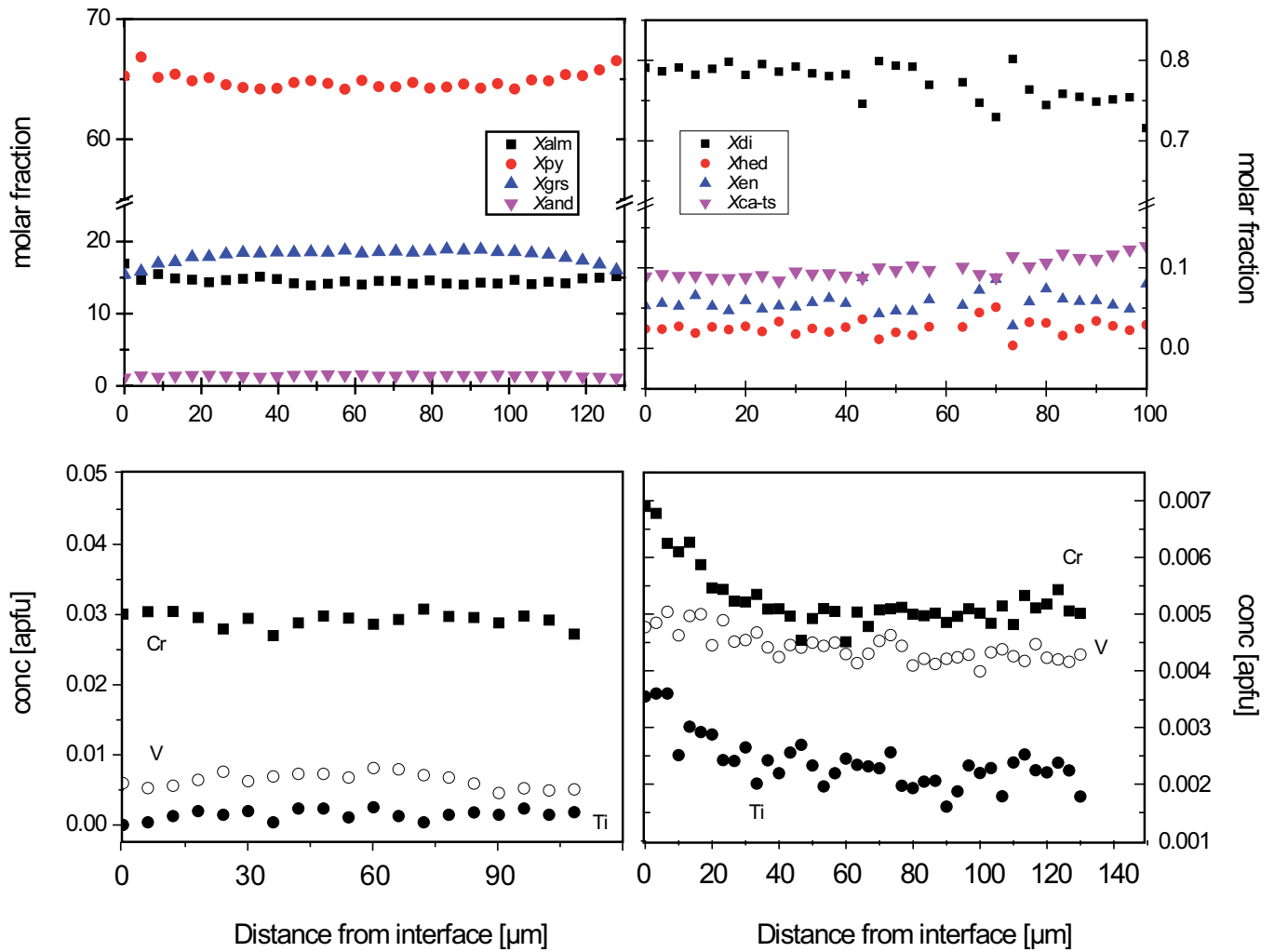


Figure 3
Müller et al.

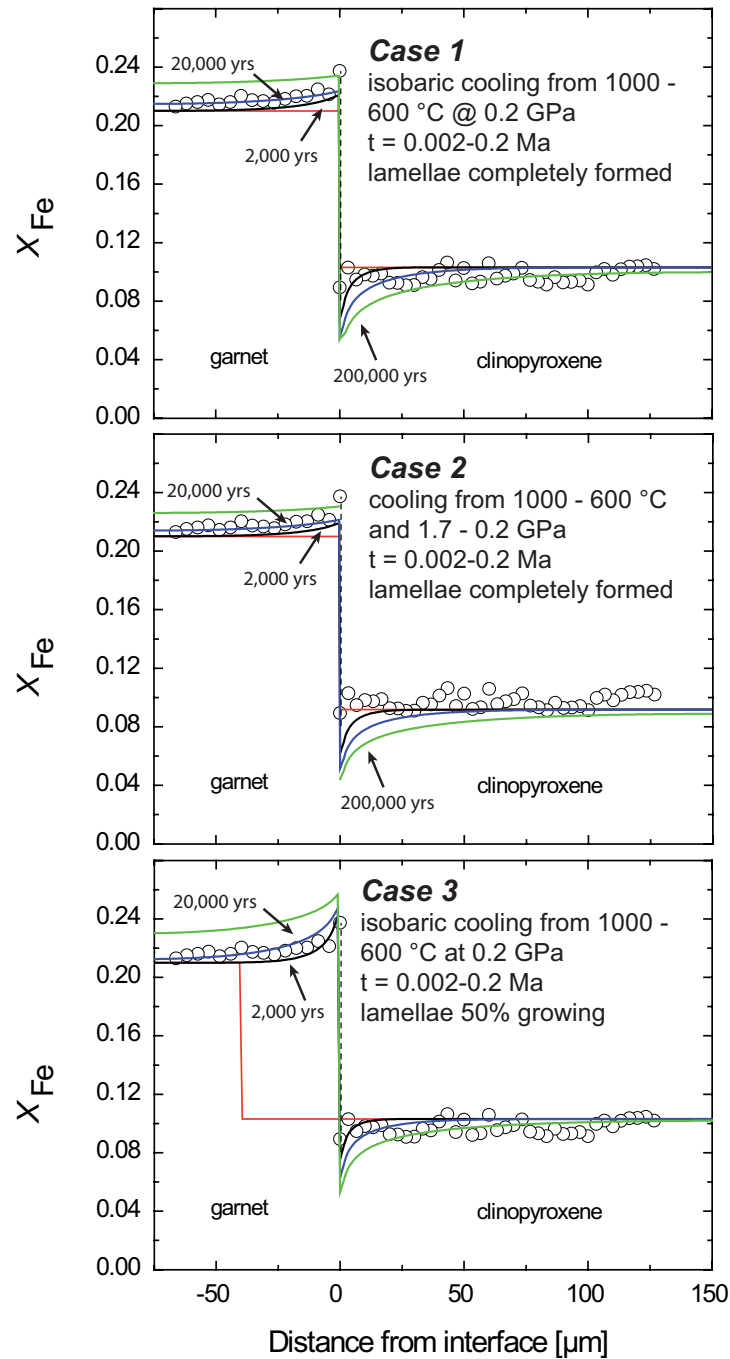


Figure 4
Müller et al.

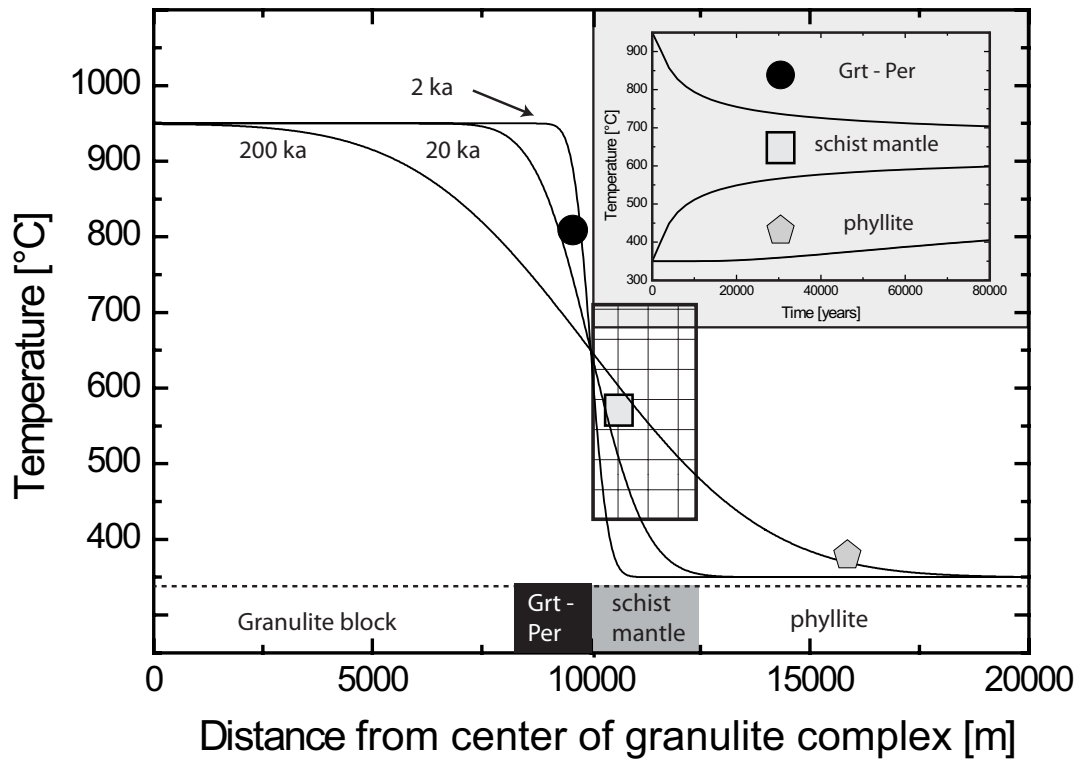
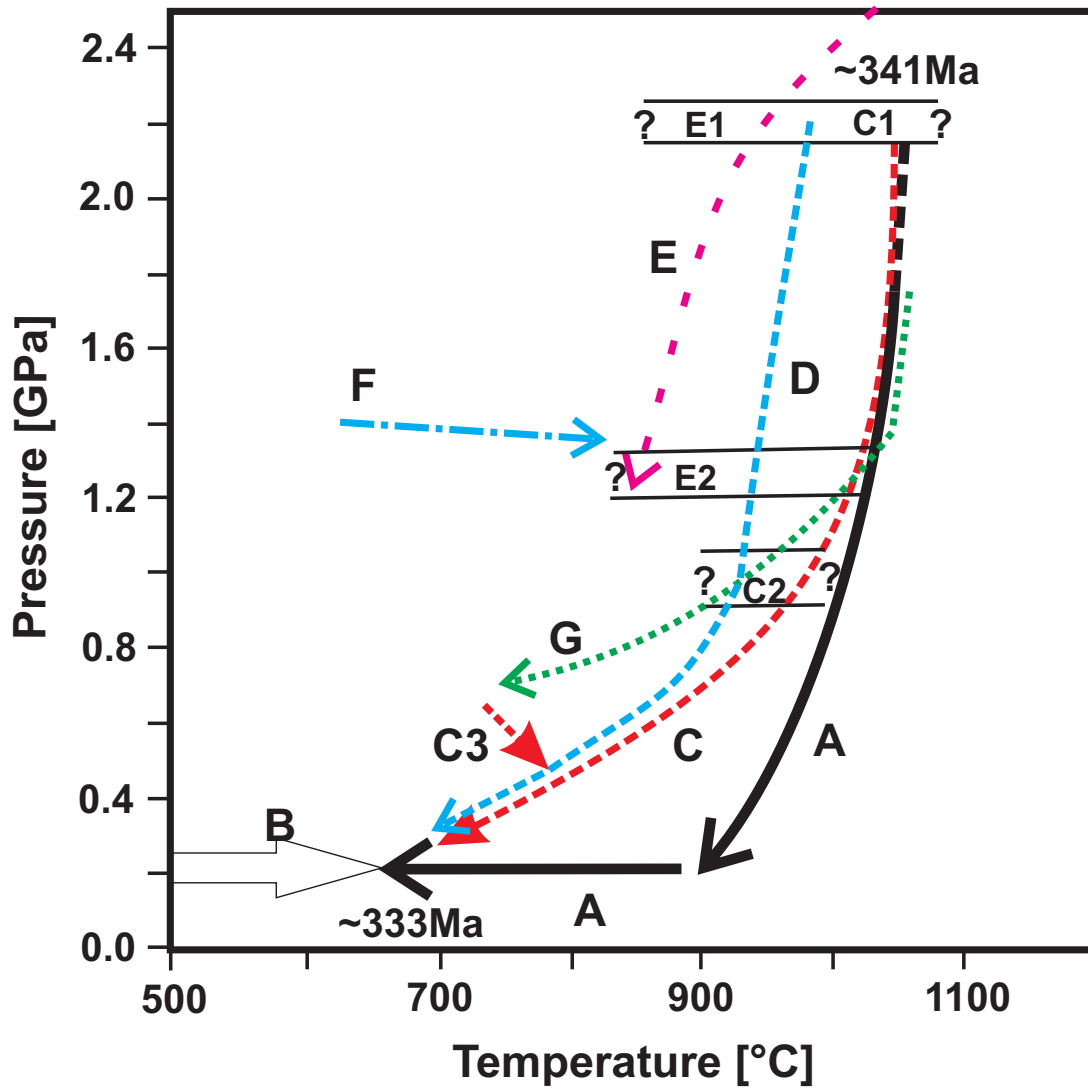


Figure 5
Müller et al.



Mueller et al.
Figure 6

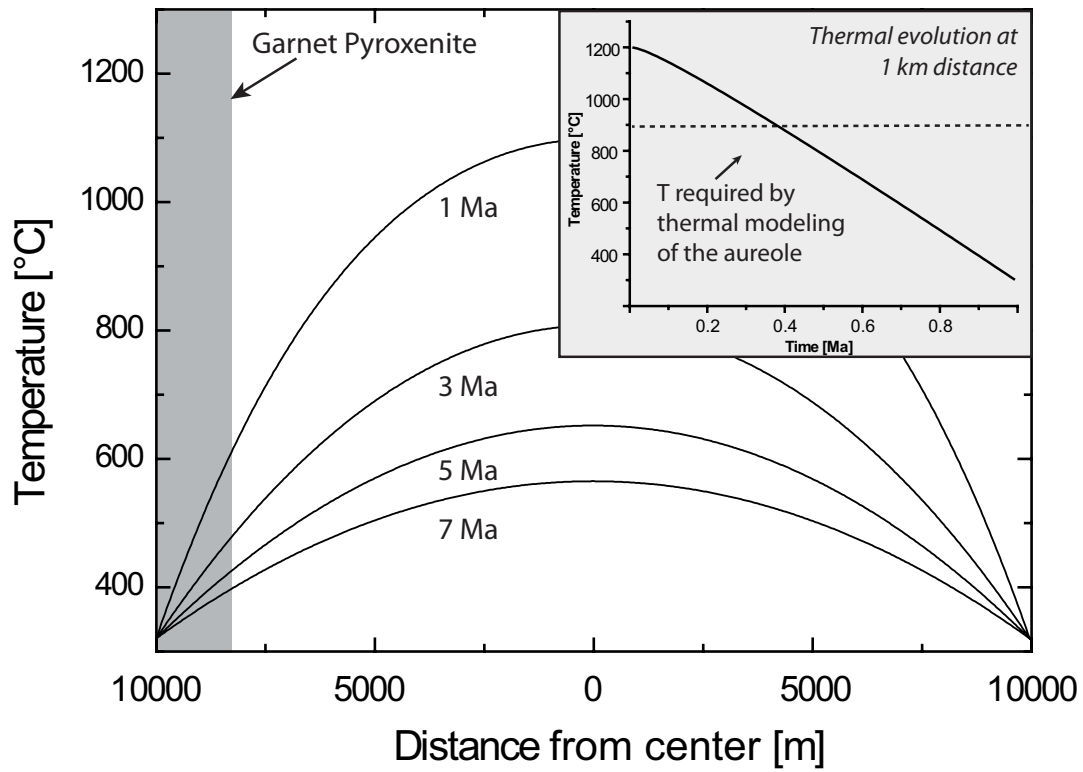


Figure 7
Müller et al.

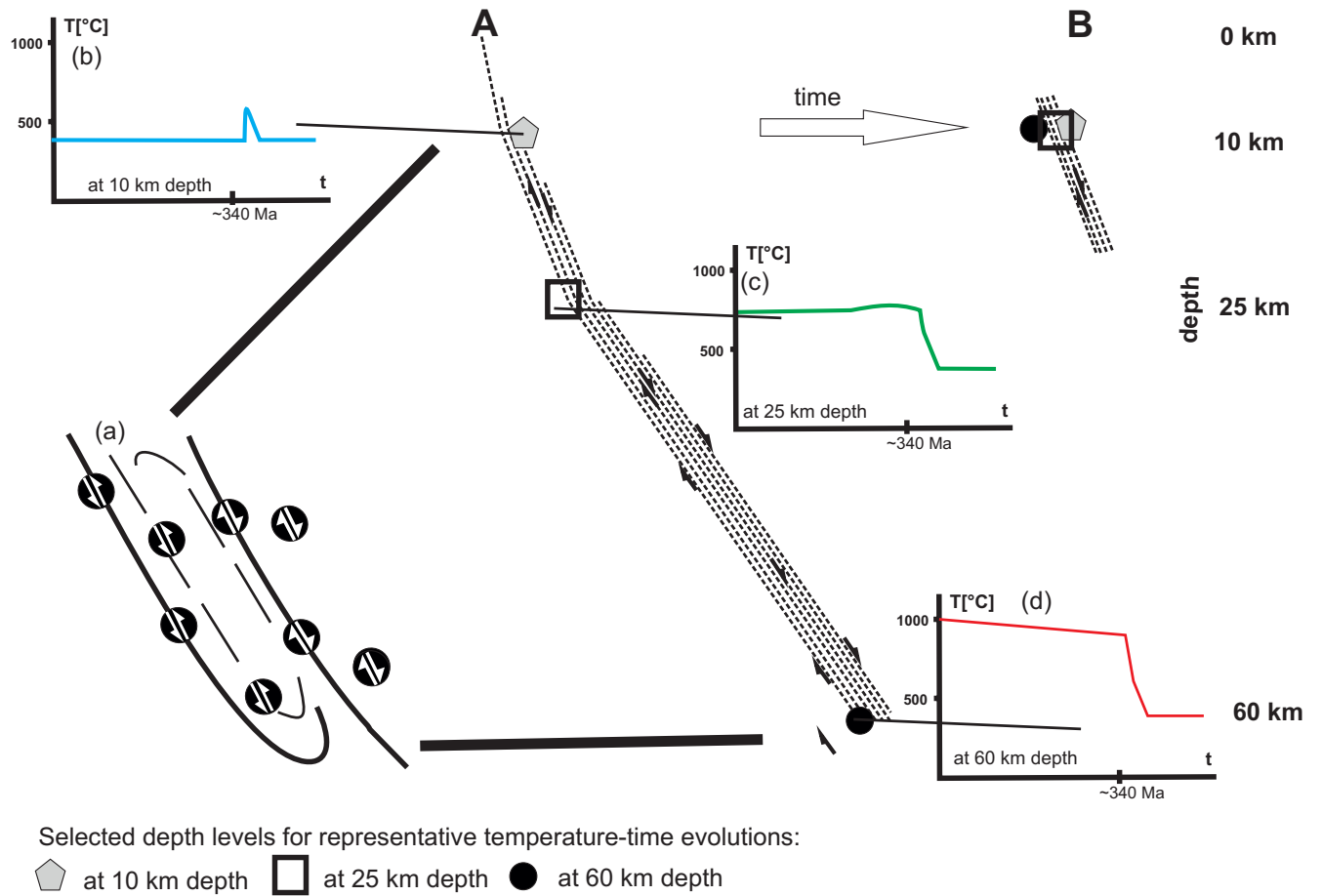


Figure 8
Mueller et al.